Lab on a Chip

Devices and applications at the micro- and nanoscale

Accepted Manuscript

This article can be cited before page numbers have been issued, to do this please use: E. Ferrarese, E. Swanekamp, T. Bui, M. J. Lazzara and C. B. Highley, *Lab Chip*, 2026, DOI: 10.1039/D5LC00219B.

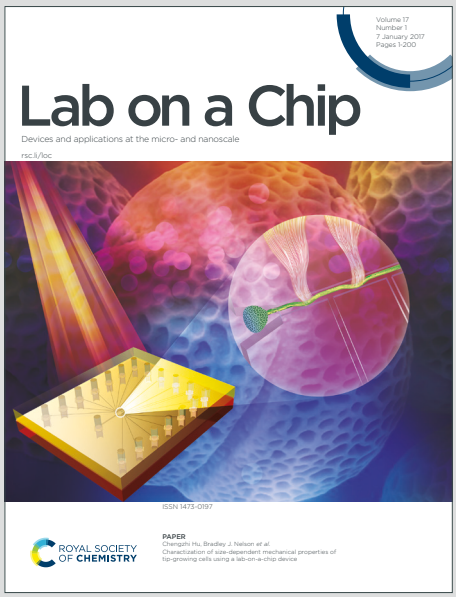

ROYAL SOCIETY OF CHEMISTRY

rsc.li/loc

View Article Online
DOI: 10.1039/D5LC00219B

Integrating Microchannels and Flows into 3D Printable Granular Hydrogel Matrices

Emily Ferrarese,[a] Emily Swanekamp,[b] Thuy-vi Bui,[b] Matthew J. Lazzara,[a,b,] and Christopher B. Highley*[a, b]

[a] Department of Chemical Engineering, University of Virginia, Charlottesville, VA 22903, USA

[b] Department of Biomedical Engineering, University of Virginia, Charlottesville, VA 22903, USA

* Email: highley@virginia.edu

Abstract

Microfluidic systems incorporating or contained within hydrogels are important in creating microphysiological systems (MPSs). Often naturally-derived hydrogels are used, as their inherent bioactivity supports dynamic cellular behaviors. Hydrogel biomaterials that are partly or fully synthetic are desirable in engineering systems with specific, designed properties, though they typically lack bioactive features of natural materials without additional molecular design. In particular, engineering synthetic biomaterials to support physiologically relevant, dynamic cellular behaviors is an important design goal. Granular hydrogels inherently permit dynamic cellular activity, owning to porosity between particles and dynamic material properties in the absence of interparticle crosslinking. However, using dynamic granular hydrogels in MPSs requires stable channels to perfuse fluid in these dynamic systems. Here, we establish channels within granular hydrogels to enable perfusion through spatially controlled interparticle crosslinking. Selective crosslinking allowed for the formation of stable channels while allowing hydrogel microparticles between two channels to remain uncrosslinked. This allowed spatiotemporal control of signals within an environment established from microparticles without interparticle crosslinking. Fluorescently tagged molecules allowed for the visualization of controlled soluble gradients between two channels within the device. Additionally, embedded 3D printing processes can be used to specify material composition within the system, demonstrating integrated technology for engineering well-defined hydrogel systems. Integrated microfluidic-based control over soluble signals in a system that is compatible with 3D printing processes will establish a basis for building MPSs for broad applications, and the ability to maintain granular systems in culture without interparticle crosslinking will enable design of synthetic hydrogels that access unique dynamic properties within these systems.

Introduction

Microfluidic technologies have enabled the creation of physiological systems that reproduce complex biology and patient-specific diseases *in vitro* within lab-on-a-chip devices.[1–3] These microphysiological systems (MPSs) can combine control over flow and control over biophysical and biochemical environments cells experience to model tissues for applications in drug discovery,[4–6] studying disease progression,[7,8] and personalized medicine[5,9,10]. As cell decisions are dependent on cells' integration of soluble and matrix-tethered biochemical signals as well as mechanical environmental cues, designing synthetic systems in well-defined hydrogels in which microflows can deliver soluble cues will present opportunities to understand and perturb physiological systems.[11,12] Microfluidic devices make it possible to establish gradients or to precisely deliver signals to cells in 2D and 3D environments.[13–15] Additionally, in establishing vascularized microphysiological models, hydrogels

View Article Online
DOI: 10.1039/D5LC00219B

integrated within microfluidic devices can contain endothelial cell-lined microfluidic channels or microvascular networks perfused by microfluidic flows.[16–20]

In microfluidic systems, natural hydrogel materials like fibrin or collagen, have been shown to readily support cellular self-organization in multicellular structures, such as microvascular networks.[12,21,22] However, fully- or partially synthetic systems are often desired to achieve designed control over material properties,[11,23] including through processing by photopatterning and photolithographic 3D printing, which allows for additional control of material compositions in microfluidic devices.[24,25] In these systems, mesoscale channels can readily be established directly in microfluidic devices by casting around needles[17,26,27] or molds[28–30], but microscale vasculature and self-organized multicellular structures typically require hydrogel design that permits cells to self-assemble. Typically compatible hydrogel design includes complex structures through crosslinks engineered to degrade[31], or respond dynamically[32] to cellular activity.

Recently, efforts using granular hydrogel biomaterials have highlighted their strengths in designing MPSs. Granular hydrogels support dynamic cellular behaviour,[33,34] microvascular structures,[35,36] and tissue growth[37,38]. Granular hydrogels are formed by packing hydrogel microparticles, whose individual diameters are typically on the order of 10 or 100s of microns, into a bulk scaffold, which results in material systems with unique properties compared to continuous hydrogels.[39,40] If microparticle-based scaffolds do not include interparticle crosslinking, or annealing,[37] the bulk material can yield and flow in response to mechanical perturbations.[36] Unlike continuous hydrogels, microparticle-based granular materials are inherently permissive; they support dynamic cellular behaviors such as proliferation, migration, or multicellular self-organization. In granular hydrogels, this is largely a function of micron size pores between individual microparticles. When particles are not crosslinked at their surfaces to one another, they also have the potential to yield and move in response to cellular activities. Granular hydrogels, made from synthetic or semi-synthetic hydrogels, are highly tunable, with control over polymer material, size, stiffness, and degradability, for example, that in turn influence cellular behaviors.[35,41–44] An additional strength of granular hydrogels in designing complex systems is their compatible with bioprinting processes that can be used to specify cellular and material architectures within these materials.[45,46]

Integrating granular hydrogels into devices in which controlled flows could be applied would allow for additional control over microenvironments presented by these materials. In particular, devices that support unannealed granular hydrogels, which lack crosslinking between microparticles, are unstable in standard *in vitro* culture.[39] Microdevices that can support unannealed granular systems would allow study of cell responses to dynamic behaviors within the microparticles that are lost after interparticle crosslinking. Additionally, devices might be designed to be compatible bioprinting processes that can be used to specify material complexity in unannealed granular hydrogels. Current examples of devices used to contain granular hydrogels rely on physical features, such as posts, to contain uncrosslinked materials.[41,47,48] As an alternative, perfusable channels embedded within granular hydrogels – which have been achieved in continuous (non-granular) hydrogels by casting the hydrogel around a removeable object[26,49,50] or material,[27,51,52] and digital light 3D printing[24] – have been established within fully annealed granular hydrogels[53–56], but are unexplored in systems in which unannealed microparticles are preserved within the granular hydrogel volume.

View Article Online
DOI: 10.1039/D5LC00219B

Our approach embeds channels fully within the biomaterial, allowing cylindrical channel topographies and avoiding the use of high aspect ratio posts or physical constraints to separate unannealed particles from flow. Here, we designed channels to align with fluidic inlets and outlets, and we used selective crosslinking of granular hydrogels immediately around a channel to stabilize the channel walls in the presence of fluid flow. These allowed hydrogel particles that comprised channel walls to be stable in the presence of shear, which might cause unannealed systems to become unpacked and dissociate into the fluid flow. However, in the space between channels, microparticles remained unannealed (**Figure 1**), allowing for them to retain their dynamic qualities in the presence of perfusive flow. The unannealed granular material could also support 3D printing processes that deposited new materials to create complex architectures within the system. By using two channels to direct flow through the device, it was thus possible to form soluble gradients within the granular hydrogel. Taken together, the system allows for unique control over both soluble cues and unique material-associated cues, the former through control over perfusion and the latter through selective annealing and 3D printing-based control over the placement of material within the microfluidic device.

Materials and methods

Norbornene modified hyaluronic acid (NorHA) synthesis

NorHA was synthesized as previously described.[57] Briefly, HA-TBA was formed by dissolving sodium hyaluronate (Lifecore, 60 kDa) in DI water and mixed with Dowex 50X proton exchange resin for 2 hours. The resulting solution was titrated with tetrabutylammonium hydroxide to pH 7, frozen and lyophilized. HA-TBA was then modified via amidation with 5-norbornene-2-methylamine, anhydrous dimethyl sulfoxide (DMSO), and benzotriazole-1-yl-oxy-tris-(dimethylamino)-phosphon-ium hexafluorophosphate (BOP) under nitrogen at room temperature for 2 h. The reaction was quenched with cold water, purified via dialysis (SpectraPor, 6–8 kDa MWCO) for 3 days with DI water and NaCl, then another 4 days with DI water, frozen and lyophilized. The degree of modification was 15.5% determined by 1H NMR (Supplemental Figure S1).

Hydrogel fabrication

A NorHA hydrogel precursor solution was made by combining NorHA (3 wt%, 0.6 thiol:norbornene (SH:Nb)), with dithiothreitol (DTT, ThermoFisher) photoinitiator lithium phenyl-2,4,6-trimethylbenzoylphosphinate (LAP, 25 mM, Sigma-Aldrich), and deionized water.

NorHA hydrogel microparticles were formed using a batch emulsification technique similar to previously reported approaches (**Figure 2**).[43] Briefly, the aqueous solution was added to light mineral oil with Span 80 (0.5 vol%, Sigma-Aldrich) at a 20:1 oil to aqueous ratio of the oil to aqueous volumes and mixed on a stir plate at 600 rpm. After 1 minute the microparticles were crosslinked under UV light (320-390 nm) at 60 $\mathrm{mW/cm^2}$ for 5 minutes. The particles were centrifuged at 3,500 rcf for 2 minutes to remove the majority of the oil and surfactant. The particles were then washed sequentially with 2 wt% Pluronic F-127 (Sigma-Aldrich), and 70 vol% ethanol two times. Microparticles were stored in phosphate buffered saline (PBS) at 4 °C until use.

View Article Online
DOI: 10.1039/D5LC00219B

Polyethylene glycol (PEG) microparticles were generated via aqueous two-phase suspension, based off previous approaches.[58] Briefly, eight arm PEG-norbornene (3 wt%, PEG-Nb, 20 kDa, JenKem), four-arm PEG-thiol (0.6 SH:Nb, 10 kDa, JenKem), and LAP (10 mM) were combined in aqueous solution. A 25 wt% solution of dextran (70 kDa, Sigma-Aldrich) was mixed with PEG-Nb hydrogel precursor solutions at a 4:1 ratio of continuous (dextran) to dispersed (PEG-Nb) phases. This mixture was mixed at 200 rpm for 1 minute prior to crosslinking under UV light at 30 $\mathrm{mW/cm^2}$ for 5 minutes. Following crosslinking, the resulting particles were suspended in 15x volume of PBS to thermodynamically favor a single-phase solution and centrifuged twice to remove dextran and other unreacted materials.

After microparticles were washed and prior to forming a bulk granular scaffold, all microparticles were allowed to swell overnight in PBS. To form granular hydrogels, microparticles were then packed together by centrifuging a suspension of microparticles at 21,000 rcf for 5 minutes and excess PBS was removed, creating packed microparticles. To allow for photoinitiated interparticle crosslinking, microparticles were resuspended in a 10 wt% PEG-SH and LAP (25 mM) crosslinking solution prior to centrifuging. Packed microparticles were loaded into an 8 mm diameter biopsy punched polydimethylsiloxane (PDMS) slab that was 5 mm think and placed under UV light for 5 minutes at 100 $\mathrm{mW/cm^2}$ to crosslink microparticles together. Granular hydrogel disks were placed in PBS at 37 °C for 24 hours to quantify stability.

Hydrogel characterization

Fluorescein isothiocyanate-dextran (FITC-dextran, 1 mg/mL, 2 MDa, Sigma-Aldrich) was added to the hydrogel precursor solution to visualize the microparticles using fluorescent microscopy in order to characterize microparticle size. Microparticles were suspended in PBS and imaged using Lecia DMi8 fluorescent widefield microscope.

Rheological behaviors of packed microparticles were characterized using oscillatory shear rheology (DHR3 rheometer, TA instruments). *For in situ* rheology the rheometer was equipped with a 20 mm sandblasted geometry and UV light at 100 mW/cm^2 was used. To determine gelation a time sweep (1 Hz, 1% strain) was performed followed by frequency sweeps (0.1-100 rads/s, 1% strain) to assess the storage and loss moduli of the hydrogel. Packed NorHA microparticles' dynamic responses to applied strain were analyzed using a 20 mm parallel plate geometry set at a gap ten times the average particle diameter. A solvent trap was used to reduce evaporation. Cyclic stain sweeps alternating between high (500%) and low (1%) strain, were used to assess the yielding and recovery responses of the packed microparticles.

Device fabrication

A computer-aided design (CAD) model of the negative mold of the device was made using Autodesk Fusion 360 software and printed using stereolithographic 3D printer (Form 2, Formlabs). The mold was washed with isopropanol twice then cured for 30 minutes at 75 °C. 27-gauge needles were inserted through the negative mold in designed locations, and PDMS (Sylgard 184, Dow Corning) was added into the reverse mold. PDMS

View Article Online
DOI: 10.1039/D5LC00219B

was cured at 37 °C for 24 hours. The PDMS device frame was then removed from the mold, plasma treated with air, and bonded to a glass coverslip (#1, 60x24 mm, VWR).

Device loading

27-gauge needles were placed through the channels of the PDMS device to template channels within the hydrogel. To form the continuous NorHA hydrogels within the device, NorHA precursor solution was added and crosslinked under UV light. Alternatively, to form a fully annealed granular hydrogel within the device, microparticles were resuspended in the crosslinking solution, then centrifuged at 21,000 rcf for 5 minutes. These packed microparticles were loaded into the PDMS device. To ensure no bubbles were formed in the material the device was carefully loaded with the packed microgels, with attention to directing deposition during pipetting to the space underneath the 27-gauge needles. With careful handling of material post-centrifugation, for example through use of a positive displacement pipette or through loading of packed material into a syringe and extruding from the syringe into the device, the introduction of air bubbles was avoided. Once the device was filled, material was crosslinked under UV light.

To form unannealed granular hydrogels containing channels, interparticle crosslinking was desired only immediately adjacent to the channels, leaving the bulk of the microparticles uncrosslinked to one another. To achieve this, LAP was localized to the needles used for templating the channels, and microparticles were resuspended in a solution containing 10 wt% PEG-SH without LAP, packed via centrifugation, and then added to the device with 27-gauge needles in place. LAP was localized to the needles by pipetting a 25 mM LAP solution over the needles after the needles were positioned within the PDMS frame and before adding the packed microparticles. Before adding packed microparticles to the device, the LAP solution was aspirated, leaving needles surfaces wetted with LAP solution. Upon adding the packed microparticles to the device, crosslinking was initiated under UV light.

In conjunction with all hydrogels used – the continuous hydrogel, the fully-annealed granular hydrogel, and the unannealed granular hydrogel – a glass coverslip (#1, 18x18 mm, VWR) was placed on top of the device immediately after loading to prevent hydrogels from drying out. Then the device was flipped and placed under UV light at 100 $\mathrm{mW/cm^2}$ for 5 minutes to crosslink the hydrogel. Then needles were slowly removed to ensure the channels were not disrupted. Devices were immediately imaged via brightfield microscopy to confirm channel formation and measure channel diameter.

Measuring channel stability

Devices were loaded with the unannealed granular hydrogel, and rhodamine B (rhodB, 12 μg/mL, Sigma-Aldrich) was injected into one of the channels at 0 h, 24 h, and 7 days for visualization of the channel to confirm stability over time. The devices were incubated at 37 °C and kept in a humid environment. The devices were rocked gently to promote flow across the device during incubation to assess prolonged flow conditions.

Diffusion characterization

View Article Online
DOI: 10.1039/D5LC00219B

Devices containing hydrogels with two parallel channels were perfused by introducing a flow of a solution fluorescently labeled albumin (FITC-albumin, 50 μg/mL, Sigma-Aldrich)[59] into one of the channels at a flow rate of 1 mL/h using a syringe pump for 25 minutes at 37 °C. Timelapse fluorescent and brightfield images were taken using Leica DMi8 widefield microscopy at 0, 5, 10, 15, 20, and 25 minutes. Due to the slow diffusion of FITC-albumin from the channel into the continuous hydrogel, the channel was perfused for 24 h at 37°C, at which point images were taken for analyzing diffusivity into the continuous hydrogel.

For dual-channel diffusion experiments, rhodB and FITC-albumin were dissolved in separate solutions, at the concentrations given above. The PDMS device was loaded, as described, with PEG-Nb packed microparticles and selectively annealed along the channels. Once the needles were removed, the FITC-albumin and rhodB solutions were introduced in solutions flowing through different parallel channels in opposite directions. Timelapse images were taken every 5 minutes of the whole device. Images including rhodB were pseudo-colored blue in figures for accessibility.

Perfusion with suspended fluorescent microspheres

Devices loaded with unnannealed NorHA microparticles were perfused with medium containing suspensions of fluorescent microspheres (FMs, FlouSpheres Carboxylate-Modified Microspheres, 10% vol/vol, ThermoFisher). FMs were 1 μm in diameter and perfused at a flow rate of 1 mL/h. Timelapse images were taken over 5 minutes.

3D printing

A biomaterial ink for 3D printing was formed from a granular hydrogel[60], based on gelatin microparticles. Gelatin microparticles were formed via a batch emulsification technique as previously described.[61] Briefly, a 15 wt% solution of gelatin type B (Sigma-Aldrich) with FITC-dextran (1 mg/mL, 2MDa, Sigma-Aldrich) was made by dissolving components at 80 °C. The warmed gelatin solution was added to warmed (80 °C) light mineral oil containing 2 vol% Span 80 and emulsified via homogenized at 2,000 rpm for 3 minutes, before being placed in a 4 °C refrigerator to cool. The resulting microparticles were washed sequentially with 2 wt% Pluronic F-127, and PBS 5 times. Gelatin microparticles were packed together at 21,000 rcf for 5 minutes to create a granular gelatin hydrogel to be used as an ink in 3D printing. A 3D printer equipped for volumetric extrusion (BIOprinter, FELIXprinter) was used print the granular gelatin ink. The granular gelatin was loaded into a syringe that was placed in the printhead for extrusion. Discrete voxels or non-linear material structures were printed into the center of unannealed NorHA packed microparticles contained within the region in the center of the device between two channels formed, as described above. Simple G-codes were used to direct the printer, and a sample is provided in the supplemental material.

Cell culture

Human umbilical vein endothelial cells (HUVEC, P6) were cultured in vascular cell basal media (ATCC) with endothelial cell medium supplements, including VEGF (ATCC), at 5% CO_2 and 37 °C in a humidified environment with media changed every 2 days. NorHA hydrogel microparticles were fabricated as described with the addition of 2 mM RGD to the precursor solution. Microparticles were sterilized with 70% ethanol and stored in media at

View Article Online
DOI: 10.1039/D5LC00219B

4 °C overnight before use. NorHA precursor solution with 2 mM RGD was sterilized by 0.22 μm filtration. Devices were sterilized in 70% ethanol. Microparticles were resuspended in PEG-SH and centrifuged at 21,000 rcf for 5 min. HUVECs were mixed within the granular hydrogel at $5x10^6$ cells/mL. For annealed granular hydrogels, 1 mM LAP was added to the particle-cell mixture. Devices were loaded and crosslinked at 15 mW/cm^2 for 60 s, after which media was added. The devices were placed on a rocker and slowly rocked to allow media to flow through the channels. After 24 h the devices were stained for viability using Live/Dead stain, calcein-AM and ethidium homodimer (Invitrogen) and fluorescently imaged to visualize the entire channels and quantify cell viability around them (Supplemental Figure S4).

Image and statistical analysis

Brightfield images of channels were analyzed to quantify channel diameter using ImageJ. Fluorescent images of diffusion were also processed and analyzed using ImageJ. To quantify diffusion from fluorescent images, intensity was traced from the channel boundary perpendicularly into the surrounding hydrogel in the device to the edge of the image. Three replicate intensity profiles were taken at different points along the channel. Axial convective flow filling the channel with fluorescent solute was significantly faster than radial diffusion. Fluorescent intensities along this trace were acquired, and background fluorescence was subtracted from each point. Each fluorescent intensity value was then normalized to the maximum fluorescent intensity value of the FITC-albumin solution in the channel. Based on the known set normalized intensity, an approximation for the effective diffusion coefficients was calculated for all hydrogel systems by taking the distance traversed by solute squared over time (equ.1).

$$D \propto \frac{Distance^2}{time} \quad \text{(eqn.1)}$$

Each diffusion experiment performed had n = 3 trials. GraphPad Prism 9 was used for all statistical analysis. Data are reported as mean ± standard error of the mean, and particle diameter is reported as mean ± standard deviation. Statistical significance was determined by a one-way ANOVA followed by a post hoc Tukey's Honest Significant Difference test. Data were graphed with the mean and error bars representing the standard deviation.

Results

Hydrogel fabrication and characterization

Hydrogel crosslinking in both continuous hydrogels and internal to hydrogel microparticles was achieved through a thiol-ene photoinitiated click chemistry reaction (Figure 2A).[62] Stoichiometric control over NorHA and DTT allowed unreacted norbornene groups to be left after crosslinking for future interparticle crosslinking, or annealing, through the same photochemistry. The NorHA microparticles generated by bulk emulsification were polydisperse with a mean diameter of 67 ± 27 μm (Figure 2B-C). Microparticles were centrifuged to pack them into a granular hydrogel. annealed, In the presence of photoinitiator, PEG-SH, and UV light, annealing between microparticles occurred rapidly (**Figure 3**A, blue line transitioning from light to dark blue to indicate gelation) within 10 – 20 s, with a slight increase in bulk storage modulus from ~100 Pa to ~120 Pa observed (Figure 3A-

View Article Online
DOI: 10.1039/D5LC00219B

B). Gelation time in a continuous NorHA precursor solution to form a continuous hydrogel (Figure 3A, green line) occurred on the same time scale. In a continuous hydrogel a significantly higher storage modulus of ~7 kPa is observed (Figure 3A-B) owing to the lack of microporosity in the bulk material.

In comparing viscoelastic properties under under static conditions or low frequency, granular and continuous hydrogels all exhibited solid-like viscoelastic properties (Supplemental Figure S2C). In the granular hydrogel system, when particles are not annealed together they retain their natural dynamic properties. Under increasing strains, the bulk microparticle material yields, exhibiting liquid-like flow. Cyclic strain sweeps that alternated between applications of low (1%) and high (500%) oscillatory strain demonstrated that the unannealed granular hydrogel had the ability to flow in response to applied strains and restabilize when strain was removed (Figure 3C), which is an important property when developing a support material for 3D printing. The potential for particles to shift and move in the absence of interparticle crosslinking also permits rearrangement to support cell activities and growth.

In characterizing the stability of the granular hydrogels, over an extended period, granular hydrogels that were annealed showed no signs of degradation after 24 h in culture, while granular hydrogels that were unannealed dissociated as microparticles eroded into the surrounding medium over this time (Figure 3E). This highlights both the potential for dynamic reorganization in unannealed systems and the critical need for systems that allow dynamic, unannealed particles to be maintained in culture, which is the focus of this work.

Device characterization

To support granular hydrogels in culture, a 3D printed negative mold (**Figure 4**A-Bi) was used to fabricate a PDMS device (Figure 4Bii-iii) that contained granular hydrogels (Figure 4Biv) with integrated microchannels (Figure 4Bv). Channels within the PDMS (Figure 4Biii) were designed to allow inlet and outlet fluidic connections to introduce controlled microflows into the hydrogels. As described above, granular hydrogels were introduced into the device and either fully annealed throughout the granular hydrogel bulk or annealed around the channels only, by localizing photoinitiator to the needles. Channel integrity was confirmed via imaging following channel formation under brightfield imaging (**Figure 5**A-C). After removing the 27-gauge needle, which had an outer diameter of 413 μm, brightfield images showed the channels had diameters of 358 ± 7 μm, 325 ± 15 μm, and 295 ± 13 μm for the bulk, fully annealed, and selectively annealed hydrogels, respectively (Figure 5D). A slight, but statistically significant, decrease in channel diameter was observed between only the selectively annealed hydrogel group and the bulk hydrogel. Channel stability was tested in the selectively annealed granular hydrogel in the device by introducing a rhodB (pseudo-colored blue) into the channel allowing for visualization the whole length of the channel over days in culture. At each of the day 0, 1 day, and 7 day timepoints, a channel is seen, evidencing long-term stability of the channel within the granular system when the microparticles are selectively annealed only adjacent to the channel and the bulk of the microparticles are unannealed (Figure 5E).

Channel stability was also observed in experiments to quantify diffusive transport from the channels. Here, medium containing fluorescently tagged albumin (FITC-albumin) was introduced in axial flow through the channels, and fluorescent imaging was used to visualize radial protein transport into the surrounding hydrogel

View Article Online
DOI: 10.1039/D5LC00219B

over time (**Figure 6**). Because the granular hdyrogels, both the annealed and selectively annealed systems, contained microporous spaces among the hydrogel microparticles, the soluble FITC-albumin was able to rapidly diffuse into the surrounding bulk material (Figure 6A-B). This interstitial diffusion supported rapid diffusive transport of this model protein granular materials' bulks in comparison to traditional, continuous hydrogels. In continuous hydrogels, the movement of soluble FITC-albumin into the hydrogel is hindered by the nanoporous polymer network, leading to no measurable diffusion after 25 min, as shown in the low normalized intensity from the channel into the hydrogel (Figure 6C).

To characterize the mass transport observed through the system, we approximated effective diffusivities from the fluorescent images. Within the continuous hydrogel system, because no measurable FITC-albumin was observed after 25 min, imaging was continued over 24 h (Supplemental Figure S3). The effective diffusion coefficient calculated for FITC-albumin in the continuous hydrogel was 8 ± 5 $\mu m^2/s$. In comparison, in the microporous granular systems the effective diffusivities observed for FITC-albumin were 303 ± 56 $\mu m^2/s$ and 319 ± 44 $\mu m^2/s$ for annealed and unannealed granular systems, respectively (Figure 6D). While there were significant differences between diffusivity measured in the granular systems compared to the continuous hydrogel, there was no significant difference between the annealed and unannealed granular hydrogels. The diffusivity (D_∞) of albumin in water at 37°C, calculated using Stokes-Einstein equation, is expected to be 106 $\mu m^2/s$ (Figure 6D, grey dashed line).[63] The observed diffusivities of albumin in the granular hydrogels were an order of magnitude greater than the observed diffusivity in the continuous hydrogel and they were on the same order of magnitude as free diffusion. However, the apparent diffusivities in the granular systems are higher than expected compared to D_∞, indicating that advective flows through the granular hydrogels must be present during experimentation as discussed below.

In addition to NorHA-based microparticles, PEG-Nb microparticles were used to form granular hydrogels to demonstrate the potential for the device to be used with, and channels to be formed in, granular hydrogels with different polymer backbones and microparticle sizes. PEG-Nb microparticles were also formulated using a phase separation process, rather than emulsification, that resulted in particles with a diameter of 12 ± 7 μm (Supplemental Figure S2). When the device was loaded with PEG-Nb microparticles and selectively crosslinked along the channel, stable channels were observed. As above, this was confirmed by continuous flow of medium through the channels that contained fluorescently labeled solutes.

To observe the potential to establish complex, multi-solute gradients within granular hydrogels, a granular hydrogel with two channels was formed within the device. RhodB, a model for a small molecule that exhibits rapid diffusion, was introduced into the top channel in the device in a flow from left to right. FITC-albumin, a model for a larger protein solute, was introduced into the bottom channel from right to left (**Figure 7**, top row: FITC-albumin in green; middle row: rhodB, pseudo-colored blue; bottom row: overlay of FITC-albumin and rhodB). The differences in diffusivity of the small rhodB molecule and larger FITC-albumin protein were readily apparent. Twenty minutes after the channels were filled rhodB had diffused across the device while the diffusive

View Article Online
DOI: 10.1039/D5LC00219B

front of the soluble FITC-albumin was still close to the main channel wall (Figure 7). After 40 minutes both gradients extended from the channel into the middle of the device (Figure 7).

To observe the movement of significantly larger suspended species, fluorescent microspheres (FMs) were perfused through the channel and timelapse imaging allowed for tracking of the FMs as they flowed through the device (Supplemental Videos 1-3). Imaging of FMs revealed flow patterns and differences in porosity between hydrogel formulations. Within the bulk hydrogel FMs were confined to the channel in which they were introduced and were not observed to move into the bulk of the hydrogel. Within the annealed and unannealed granular hydrogel groups, FMs were observed moving with convective flow along the channel length and into the surrounding granular hydrogel system. From this experimentation and diffusion experiments, described above, it was evident both that soluble and suspended particles could easily be transported into the bulk granular system, but also that when axial flows were initiated in the channels, the change in pressure upon initiating convection into the device drove radial flows from the channel in the microporous granular systems. This carried fluorescent solutes, above, and FMs, here, with the radial flow. Pore spaces between microparticles within granular hydrogels were thus able to support convection into the bulk of the material.

3D printing

To establish that 3D printing processes could be used to design heterogeneous material architectures between channels within a microdevice, we printed a biomaterial ink directly into the unannealed microparticles within a selectively annealed device prior to closing the device. In the selectively annealed systems, where crosslinking only occurred between microparticles adjacent to the channels, the unannealed microparticles in the bulk of the granular hydrogel flowed around the printer nozzle (schematic in Figure 1) in an embedded 3D printing process on chip. To demonstrate the potential for using 3D printing to establish material complexity, both discrete features and non-linear structures were formed in the system. First, discrete voxels were printed in the center region of the device (**Figure 8**A). According to the computer design and print parameters, the gelatin microparticle voxels that were printed were about 1.5 mm in diameter. Voxels were positioned with 4 mm or 2 mm between centers. Next, a sawtooth patterns with a 1 mm (Figure 8B) or 1.5 mm (Figure 8C) amplitude and 3 mm frequency were printed. The larger print (Figure 8C) was in contact with a surrounding channel, allowing transport of liquefied gelatin to be visualized from the printed ink into the channel, and then axially along the channel (Figure 8C).

Cells within hydrogels on-device

To demonstrate the strengths of channels within granular hydrogels in supporting cell viability within devices, endothelial cells (HUVECs) were cultured within the device in either selectively annealed granular hydrogels, fully annealed granular hydrogels, or continuous hydrogels for 24 h (**Figure 9**). After 24 h cells within the continuous hydrogel had low cell viabilities within the hydrogel, compared to cells in the granular hydrogels (Figure 9B). Cell viability was only 22.2 for the continuous hydrogel, but 79.8% and 78.2% for the fully annealed and selectively annealed granular hydrogels, respectively.

Discussion

View Article Online
DOI: 10.1039/D5LC00219B

Advances in microphysiological systems and *in vitro* tissue models will benefit from systems where it is possible to establish complex material compositions of material, and control critical soluble and matrix bound signals. Granular hydrogels facilitate the design of material complexity that is not available in continuous bulk hydrogels through inherent features like microporosity and their discrete particulate nature[39] as well as compatibility with embedded printing processes.[64–66] The development of a microfluidic system that integrates channels within granular materials will allow control of soluble signals within granular systems and will allow studies in granular hydrogels without unannealed microparticles dissociating into surrounding media. This technology would support maintenance of systems with highly dynamic properties over time and under perfusion, enabling new cell-material interactions to be designed via dynamic microenvironmental cues. Additionally, a device compatible with 3D printing presents opportunities for controlling combined soluble and physical signals.

Granular hydrogels were formed from norbornene-modified hyaluronic acid (HA) and polyethylene-glycol (PEG) microparticles (Figure 2 and Supplemental Figure S2). Stoichiometric control of norbornene functionalization allows design of physical and biochemical functionalities in hydrogels[62,67] and facilitates interparticle crosslinking in granular systems.[68,69] This control was leveraged here to design systems with excess norbornene groups to facilitate interparticle crosslinking adjacent to channels to stabilize granular hydrogels around the channel lumen, while leaving the bulk of the granular system uncrosslinked. Packed microparticle systems that lack interparticle crosslinking retain the ability for individual microparticles to move past one another, preserving inherent stress yielding properties within granular materials that can be challenging to achieve without careful molecular design in continuous bulk hydrogels (Figure 3). These dynamic behaviors can be seen in the rheological transitions between solid- and liquid-like behaviors in uncrosslinked granular systems to applied strains (Figure 3D). These properties are desirable in allowing bioprinting to control material architectures[60] and stress yielding matrices can influence cell responses[70]. However, unannealed granular systems dissociate in culture environments without interparticle crosslinking (Figure 3D) in the absence of a device designed to retain them.

To address this challenge, here we developed a PDMS of a microfluidic device to contain granular hydrogels and allow for introduction of controlled flows. The simple fabrication of this device using of a 3D-printer allowed for a low-cost entry point to for initial engineering and ultimately design of the device for specific applications. Additionally, additive manufacturing technology could be used for higher throughput fabrication of these systems and additional fluidic control systems or devices multiplexed on a single chip would enable easy scale up for translational applications addressing clinical needs in personalized models. Here, these systems supported granular hydrogels with channels aligned to fluidic inputs. Particles forming channel walls were locally stabilized by interparticle crosslinking, allowing flow while leaving the bulk of the granular system unannealed. The approach here achieved this by localizing photoinitiator to a small volume of solution wetting channel-forming needles. Diffusion-based approaches have been used elsewhere to spatially control crosslinking near 3D printed structures.[71]

The open device design used here allows for materials to be introduced into the device, with materials fully surrounding channel forming needles. To avoid bubble formation, granular hydrogels should be centrifuged fully for packing and extruded from the bottom surface upwards into the device. While careful deposition of granular

View Article Online
DOI: 10.1039/D5LC00219B

hydrogels avoids entrapping air in deposited hydrogels, if a material gap forms, light centrifugation of the device prior closing can collapse voids. Bubbles during perfusion have the potential to disturb the granular support surrounding channels, so microfluidic connections should be made to air-free feeds. With air free and steady flows, channels granular systems, but fully annealed and selectively annealed, supported flow and remained patent for days (Figure 5E). Channel diameters were specified by needle templating (Figure 5D, grey dash line), which yielded channels whose diameter became modestly smaller due to swelling of the hydrogels after needle removal. Swelling increased as total crosslinking within the hydrogels decreased, as expected. Continuous hydrogels exhibited the smallest changes to channel diameters and unannealed granular hydrogels the greatest. Importantly, while swelling must be accounted for in planning an application, swelling did not disrupt channel stability over time (Figure 5E). The granular hydrogels and devices used are expected to be compatible with other channel-formation process, including removable 3D printed ink used to template vessel structures.[52,72–74]

Gradients of soluble molecules were established from channels in granular hydrogels. Transport of FITC-albumin into the granular hydrogels, where one channel served as a source of the protein and the other as a sink, evidenced rapid transport of FITC-albumin through the materials' bulks. Transport of the labeled protein extended far into the material surrounding the channels after 25 min of observation, which contrasted with continuous hydrogels (Figure 6A). Within continuous hydrogels, the formation of a protein gradient required hours (Supplemental Figure S3). Granular systems can thus address avoid challenges faced by continuous hydrogel systems in supporting rapid transport and quick changes of soluble signals, primarily due to the lack of microporosity that might support convection or free diffusion, with transport instead occurring through nanoporosity in the continuous polymer network. Rapid gradient formation is expected to be useful in spatiotemporal control or switching of signals important to an MPS and will also be of value where soluble signals with short half-lives are important in understanding physiological processes.

Towards quantitative understanding of transport informing the design of spatiotemporal signaling, apparent diffusivities for FITC-albumin in the hydrogel system were quantified (Figure 6D). Apparent diffusivities of FITC-albumin evidenced the same order of magnitude as in water (indicated by the gray dashed line in Figure 6D)[63], which is unsurprising due to the microscale interstitial spaces between particles where nanoscale solute diffusion is rapid and uninhibited. The apparent diffusivity of FITC-albumin in the granular hydrogel was, however, three times greater than the value calculated for free diffusion using the Stokes-Einstein relationship, indicating that transport observed in the device was not solely due to diffusion. It is likely that advection into the material contributed to transport as flows initiating the starts of experiments created small pressure imbalances. Additional observations of flow using FMs confirmed that the granular system easily supported interstitial flow and the transport of much larger, microscale particles. While the system's ability to support transport is a potential strength, future development of the microfluidic device should include refinements to controlling the introduction of flows and pressure during experiments, for example through refining device packaging and fluidic connections. A more precise quantitative model of solute diffusion in the granular system should account for interstitial flow rates, material porosity, and potentially nanoscale porosity within the microparticles.

View Article Online
DOI: 10.1039/D5LC00219B

In reciprocal cell-microenvironment interactions within physiological systems, complex extracellular signals are integrated through cell signaling pathways to determine cellular behavior. Towards demonstrating the potential to define multiple soluble signaling gradients, two model molecules, rhodB and FITC-albumin, were introduced to the granular system and they established opposing concentration gradients (Figure 7A) across the granular bulk, as expected from diffusion studies. Each channel within the device acted as the source for one compound and the sink for the other. Additionally, towards demonstrating generalizability of granular systems in microdevices to different backbone materials, here small (~10 μm in diameter) PEG-Nb microparticles were employed. As with NorHA, hydrogel channels were stable and gradients formed rapidly, indicating that integrating and perfusing channels within granular hydrogels could be used with a range of microparticle sizes and with both natural- derived and synthetic polymers.

We also expected, based on granular hydrogels' microporosity and the calculations of apparent diffusivity, that granular hydrogels were supporting interstitial flows. This might be a strength in models of disease and physiological systems, were interstitial flows are important in cancer metastasis[7] and microvascular network formation[18,21,28]. The presence of radial flow from the channels and into the granular systems' interstitial spaces was directly observed through the inclusion of FMs (Supplemental Videos 1-3) that were carried in suspension in flow into the granular materials' interstitial spaces. Because of their large, microscale size relative to molecular solutes, convection of FMs also suggests the potential for cellular movement within such a granular hydrogel, highlighting the biological attraction of these materials in modeling dynamic cell behaviors and the need for culture systems that allow researchers to exploit these features in designing synthetic cellular matrices.

Towards designing complex material structures in addition to soluble signaling, this system allowed 3D printing to be used to control material heterogeneities within the granular hydrogel on the microdevice. Controlling crosslinking of microparticles to one another adjacent to the channels allowed for the granular hydrogel between the channels to be used as a support bath for 3D printing. The unannealed granular space then supported deposition of printed material in complex structures on the microdevice (Figure 8). These included the specific and regular computer-guided placement of the depots of a granular gelatin material and the printing of a non-linear sawtooth structure in the granular bulk between the two channels that would be challenging to introduce into an MPS system. Unlike a continuous hydrogel system, the granular hydrogel can support this embedded printing, which can be extended to allow depositions of materials with different mechanics, bio-functionalities, and porosities.[39] Additionally, bioprinting can help create biological systems that have controlled placement of cells and materials within the microfluidic device, which will be valuable for reproducible control of biological environments and emergent structures. To illustrate the patency of channels surrounding a printed structure and also the enhanced diffusion within their mesoscale diameters, a gelatin bioink that melted upon heating was printed so that one end of the filament was in contact with the channel. Upon melting, diffusion into the channel and along its length was observed in fluorescent imaging (Figure 8C).

Finally, culturing cells within granular hydrogel allows for higher viability. The nanoscale porosity of continuous hydrogel slows transport and limits the ability for cells to spread and grow within the hydrogel, without further design of the material for degradation. In a continuous system we observed a substantial loss viability after 24 h

View Article Online
DOI: 10.1039/D5LC00219B

in continuous gels (Figure 9). The inherent microporosity with granular hydrogels allows cells to reside and move within microporous interstitial spaces among the particles without additional molecular design. Additionally, it enhances transport, as discussed. Consequently, cell culture in granular hydrogels significantly increased the viability of HUVECs in devices after 24 h. Importantly, because we were able to culture cells within selectively annealed microgels, there are new opportunities for studying complex biophysical cues and cellular responses. Compared to annealed granular systems, unannealed systems offer environments where unannealed particles might move in response to forces. But culture unannealed systems is challenging, as they erode in standard tissue culture systems. This system addresses this challenge and enables control over soluble signaling gradients and matrix architectures, the integration of microfluidics, and supports embedded printing to facilitate design of a range of cell-instructive cues not available in other systems. This device is expected to support applications of controlled flows to granular systems that will facilitate the development of well-defined biomaterial systems *in vitro* and of advanced models for tissue engineering and microphysiological applications.

Conclusion

In this work, a microfluidic device was developed to contain granular hydrogels, with the ability to selectively crosslink microparticles adjacent to channels within the device, leaving microparticles in the hydrogel volume between the channels uncrosslinked to one another. These unannealed granular hydrogels have valuable properties but are otherwise challenging to be used as scaffolds for tissue engineering or microphysiological systems because they undergo erosion into culture media. Here, a device that facilitated easy loading of packed microparticles allowed the fabrication of channels into which media could be introduced, without scaffold erosion. Through spatial control over crosslinking that locally stabilized channels, gradients of soluble compounds could be established across the hydrogels. Additionally, the uncrosslinked microparticles could support material to deposition via 3D printing in the device bulk. Taken together, the system enabled the design and presentation of diverse matrix-bound and soluble cues that might be presented to cells, which also grew better within granular materials than in continuous hydrogels. Granular hydrogels thus supported a combined microfluidic and 3D-printing approach for exerting spatiotemporal control over soluble and material-based signals in dynamic systems. Looking forward, the system will allow increased complexity to be designed into biological systems *in vitro* for a variety of biomedical applications.

Conflicts of interest

There are no conflicts to declare.

Data availability

The data supporting these findings is available in Supplementary Information. Additional data is available upon request from the corresponding author.

Acknowledgements

View Article Online
DOI: 10.1039/D5LC00219B

This research was supported by supported by NIGMS R35 GM147410.

References

1 K. Yum, S. G. Hong, K. E. Healy and L. P. Lee, *Biotechnol. J.*, 2014, **9**, 16–27.

2 M. F. Peters, A. L. Choy, C. Pin, D. J. Leishman, A. Moisan, L. Ewart, P. J. Guzzie-Peck, R. Sura, D. A. Keller, C. W Scott and K. L. Kolaja, *Lab. Chip*, 2020, **20**, 1177–1190.

3 M. L. Ewald, Y.-H. Chen, A. P. Lee and C. C. W. Hughes, *Lab. Chip*, 2021, **21**, 3244–3262.

4 E. W. Esch, A. Bahinski and D. Huh, *Nat. Rev. Drug Discov.*, 2015, **14**, 248–260.

5 D. E. Ingber, *Nat. Rev. Genet.*, 2022, **23**, 467–491.

6 Y. I. Wang, C. Carmona, J. J. Hickman and M. L. Shuler, *Adv. Healthc. Mater.*, 2018, **7**, 1701000.

7 J. M. Munson and A. C. Shieh, *Cancer Manag. Res.*, 2014, **6**, 317–328.

8 K. Nichols, R. Koppes and A. Koppes, *Curr. Opin. Biomed. Eng.*, 2020, **14**, 42–51.

9 K. Boylin, G. V. Aquino, M. Purdon, K. Abedi, M. Kasendra and R. Barrile, *Biofabrication*, 2024, **16**, 032007.

10 M. Tran, C. Heo, L. P. Lee and H. Cho, *Biomater. Res.*, 2022, **26**, 82.

11 I. M. El-Sherbiny and M. H. Yacoub, *Glob. Cardiol. Sci. Pract.*, 2013, **2013**, 38.

12 C. J. Bettinger and J. T. Borenstein, *Soft Matter*, 2010, **6**, 4999–5015.

13 S. An, S. Y. Han and S.-W. Cho, *BioChip J.*, 2019, **13**, 306–322.

14 S. Sant, M. J. Hancock, J. P. Donnelly, D. Iyer and A. Khademhosseini, *Can. J. Chem. Eng.*, 2010, **88**, 899–911.

15 T. M. Keenan and A. Folch, *Lab. Chip*, 2007, **8**, 34–57.

16 K. H. Song, C. B. Highley, A. Rouff and J. A. Burdick, *Adv. Funct. Mater.*, 2018, **28**, 1801331.

17 W. Y. Wang, R. N. Kent, S. A. Huang, E. H. Jarman, E. H. Shikanov, C. D. Davidson, H. L. Hiraki, D. Lin, M. A. Wall, D. L. Matera, J.-W. Shin, W. J. Polacheck, A. Shikanov and B. M. Baker, *Acta Biomater.*, 2021, **135**, 260–273.

18 A. Reinitz, J. DeStefano, M. Ye, A. D. Wong and P. C. Searson, *Microvasc. Res.*, 2015, **99**, 8–18.

19 Y. Nashimoto, T. Hayashi, I. Kunita, A. Nakamasu, Y. Torisawa, M. Nakayama, H. Takigawa-Imamura, H. Kotera, K. Nishiyama, T. Miura and R. Yokokawa, *Integr. Biol.*, 2017, **9**, 506–518.

20 K. A. Homan, N. Gupta, K. T. Kroll, D. B. Kolesky, M. Skylar-Scott, T. Miyoshi, D. Mau, M. T. Valerius, T. Ferrante, J. V. Bonventre, J. A. Lewis and R. Morizane, *Nat. Methods*, 2019, **16**, 255–262.

21 I. K. Zervantonakis, S. K. Hughes-Alford, J. L. Charest, J. S. Condeelis, F. B. Gertler and R. D. Kamm, *Proc. Natl. Acad. Sci.*, 2012, **109**, 13515–13520.

22 S. Kim, H. Lee, M. Chung and N. Li Jeon, *Lab. Chip*, 2013, **13**, 1489–1500.

23 A. K. Gaharwar, I. Singh and A. Khademhosseini, *Nat. Rev. Mater.*, 2020, **5**, 686–705.

24 A. K. Miri, D. Nieto, L. Iglesias, H. Goodarzi Hosseinabadi, S. Maharjan, G. U. Ruiz-Esparza, P. Khoshakhlagh, A. Manbachi, M. R. Dokmeci, S. Chen, S. R. Shin, Y. S. Zhang and A. Khademhosseini, *Adv. Mater.*, 2018, **30**, 1800242.

View Article Online
DOI: 10.1039/D5LC00219B

25 B. M. Gillette, J. A. Jensen, B. Tang, G. J. Yang, A. Bazargan-Lari, M. Zhong and S. K. Sia, *Nat. Mater.*, 2008, **7**, 636–640.

26 W. Y. Wang, D. Lin, E. H. Jarman, W. J. Polacheck and B. M. Baker, *Lab. Chip*, 2020, **20**, 1153–1166.

27 J. S. Miller, K. R. Stevens, M. T. Yang, B. M. Baker, D.-H. T. Nguyen, D. M. Cohen, E. Toro, A. A. Chen, P. A. Galie, X. Yu, R. Chaturvedi, S. N. Bhatia and C. S. Chen, *Nat. Mater.*, 2012, **11**, 768–774.

28 J. A. Whisler, M. B. Chen and R. D. Kamm, *Tissue Eng. Part C Methods*, 2014, **20**, 543–552.

29 L. L. Bischel, E. W. K. Young, B. R. Mader and D. J. Beebe, *Biomaterials*, 2013, **34**, 1471–1477.

30 N. W. Choi, M. Cabodi, B. Held, J. P. Gleghorn, L. J. Bonassar and A. D. Stroock, *Nat. Mater.*, 2007, **6**, 908–915.

31 J. J. Moon, J. E. Saik, R. A. Poché, J. E. Leslie-Barbick, S.-H. Lee, A. A. Smith, M. E. Dickinson and J. L. West, *Biomaterials*, 2010, **31**, 3840–3847.

32 Z. Wei, R. Schnellmann, H. C. Pruitt and S. Gerecht, *Cell Stem Cell*, 2020, **27**, 798-812.e6.

33 S. Xin, C. A. Gregory and D. L. Alge, *Acta Biomater.*, 2020, **101**, 227–236.

34 A. S. Caldwell, V. V. Rao, A. C. Golden and K. S. Anseth, *Biomaterials*, 2020, **232**, 119725.

35 Z. Ataie, S. Horchler, A. Jaberi, S. V. Koduru, J. C. El-Mallah, M. Sun, S. Kheirabadi, A. Kedzierski, A. Risbud, A. R. A. E. Silva, D. J. Ravnic and A. Sheikhi, *Small*, 2024, **20**, 2307928.

36 T. H. Qazi, V. G. Muir and J. A. Burdick, *ACS Biomater. Sci. Eng.*, 2022, **8**, 1427–1442.

37 D. R. Griffin, W. M. Weaver, P. O. Scumpia, D. Di Carlo and T. Segura, *Nat. Mater.*, 2015, **14**, 737–744.

38 L. J. Pruett, C. H. Jenkins, N. S. Singh, K. J. Catallo and D. R. Griffin, *Adv. Funct. Mater.*, 2021, **31**, 2104337.

39 A. C. Daly, L. Riley, T. Segura and J. A. Burdick, *Nat. Rev. Mater.*, 2020, **5**, 20–43.

40 A. C. Daly, *Adv. Healthc. Mater.*, 2023, **n/a**, 2301388.

41 L. A. Krattiger, D. B. Emiroglu, S. Pravato, L. O. Moser, O. A. Bachmann, S. Y. La Cioppa, G. J. R. Rivera, J. A. Burdick, A. J. deMello, M. W. Tibbitt and M. Ehrbar, *Adv. Funct. Mater.*, 2024, **n/a**, 2310507.

42 C. E. Miksch, N. P. Skillin, B. E. Kirkpatrick, G. K. Hach, V. V. Rao, T. J. White and K. S. Anseth, *Small*, 2022, **18**, 2200951.

43 V. G. Muir, T. H. Qazi, J. Shan, J. Groll and J. A. Burdick, *ACS Biomater. Sci. Eng.*, 2021, **7**, 4269–4281.

44 V. G. Muir, S. Weintraub, A. P. Dhand, H. Fallahi, L. Han and J. A. Burdick, *Adv. Sci.*, 2023, **n/a**, 2206117.

45 Z. Ataie, S. Kheirabadi, J. W. Zhang, A. Kedzierski, C. Petrosky, R. Jiang, C. Vollberg and A. Sheikhi, *Small*, 2022, **18**, 2202390.

46 S. Xin, K. A. Deo, J. Dai, N. K. R. Pandian, D. Chimene, R. M. Moebius, A. Jain, A. Han, A. K. Gaharwar and D. L. Alge, *Sci. Adv.*, 2021, **7**, eabk3087.

47 A. P. McGuigan and M. V. Sefton, *J. Tissue Eng. Regen. Med.*, 2007, **1**, 136–145.

48 A. P. McGuigan and M. V. Sefton, *Proc. Natl. Acad. Sci.*, 2006, **103**, 11461–11466.

49 J. A. Kim, H. N. Kim, S.-K. Im, S. Chung, J. Y. Kang and N. Choi, *Biomicrofluidics*, 2015, **9**, 024115.

View Article Online
DOI: 10.1039/D5LC00219B

50 J. Paek, S. E. Park, Q. Lu, K.-T. Park, M. Cho, J. M. Oh, K. W. Kwon, Y. Yi, J. W. Song, H. I. Edelstein, J. Ishibashi, W. Yang, J. W. Myerson, R. Y. Kiseleva, P. Aprelev, E. D. Hood, D. Stambolian, P. Seale, V. R. Muzykantov and D. Huh, *ACS Nano*, 2019, **13**, 7627–7643.

51 M. A. Skylar-Scott, S. G. M. Uzel, L. L. Nam, J. H. Ahrens, R. L. Truby, S. Damaraju and J. A. Lewis, *Sci. Adv.*, 2019, **5**, eaaw2459.

52 D. B. Kolesky, K. A. Homan, M. A. Skylar-Scott and J. A. Lewis, *Proc. Natl. Acad. Sci.*, 2016, **113**, 3179–3184.

53 A. M. Compaan, K. Song, W. Chai and Y. Huang, *ACS Appl. Mater. Interfaces*, 2020, **12**, 7855–7868.

54 T. G. Molley, G. K. Jalandhra, S. R. Nemec, A. S. Tiffany, A. Patkunarajah, K. Poole, B. A. C. Harley, T. Hung and K. A. Kilian, *Biomater. Sci.*, 2021, **9**, 4496–4509.

55 A. J. Seymour, S. Shin and S. C. Heilshorn, *Adv. Healthc. Mater.*, 2021, **10**, 2100644.

56 J. Kajtez, M. F. Wesseler, M. Birtele, F. R. Khorasgani, D. Rylander Ottosson, A. Heiskanen, T. Kamperman, J. Leijten, A. Martínez-Serrano, N. B. Larsen, T. E. Angelini, M. Parmar, J. U. Lind and J. Emnéus, *Adv. Sci.*, 2022, **9**, 2201392.

57 S. L. Vega, M. Y. Kwon, K. H. Song, C. Wang, R. L. Mauck, L. Han and J. A. Burdick, *Nat. Commun.*, 2018, **9**, 614.

58 A. K. Fraser, C. S. Ki and C.-C. Lin, *Macromol. Chem. Phys.*, 2014, **215**, 507–515.

59 A. Shkilnyy, P. Proulx, J. Sharp, M. Lepage and P. Vermette, *Colloids Surf. B Biointerfaces*, 2012, **93**, 202–207.

60 C. B. Highley, K. H. Song, A. C. Daly and J. A. Burdick, *Adv. Sci.*, 2019, **6**, 1801076.

61 J. Whitewolf, L. Riley, B. Brady, G. Grewal, T. Segura and C. Highley, *bioRxiv*, 2024, preprint, DOI: 10.1101/2024.10.28.620615.

62 B. D. Fairbanks, M. P. Schwartz, A. E. Halevi, C. R. Nuttelman, C. N. Bowman and K. S. Anseth, *Adv. Mater.*, 2009, **21**, 5005–5010.

63 E. M. Johnson, D. A. Berk, R. K. Jain and W. M. Deen, *Biophys. J.*, 1996, **70**, 1017–1023.

64 T. Bhattacharjee, S. M. Zehnder, K. G. Rowe, S. Jain, R. M. Nixon, W. G. Sawyer and T. E. Angelini, *Sci. Adv.*, 2015, **1**, e1500655.

65 T. Bhattacharjee, C. J. Gil, S. L. Marshall, J. M. Urueña, C. S. O'Bryan, M. Carstens, B. Keselowsky, G. D. Palmer, S. Ghivizzani, C. P. Gibbs, W. G. Sawyer and T. E. Angelini, *ACS Biomater. Sci. Eng.*, 2016, **2**, 1787–1795.

66 T. J. Hinton, Q. Jallerat, R. N. Palchesko, J. H. Park, M. S. Grodzicki, H.-J. Shue, M. H. Ramadan, A. R. Hudson and A. W. Feinberg, *Sci. Adv.*, 2015, **1**, e1500758.

67 W. M. Gramlich, I. L. Kim and J. A. Burdick, *Biomaterials*, 2013, **34**, 9803–9811.

68 S. Xin, O. M. Wyman and D. L. Alge, *Adv. Healthc. Mater.*, 2018, **7**, 1800160.

69 N. J. Darling, W. Xi, E. Sideris, A. R. Anderson, C. Pong, S. T. Carmichael and T. Segura, *Adv. Healthc. Mater.*, 2020, **9**, 1901391.

70 Y. Ma, T. Han, Q. Yang, J. Wang, B. Feng, Y. Jia, Z. Wei and F. Xu, *Adv. Funct. Mater.*, 2021, **31**, 2100848.

71 B. Cai, D. Kilian, D. Ramos Mejia, R. J. Rios, A. Ali and S. C. Heilshorn, *Adv. Sci.*, 2024, **11**, 2306470.

View Article Online
DOI: 10.1039/D5LC00219B

72 A. J. Seymour, A. D. Westerfield, V. C. Cornelius, M. A. Skylar-Scott and S. C. Heilshorn, *Biofabrication*, 2022, **14**, 022002.

73 W. Wu, A. DeConinck and J. A. Lewis, *Adv. Mater.*, 2011, **23**, H178–H183.

74 C. B. Highley, C. B. Rodell and J. A. Burdick, *Adv. Mater.*, 2015, **27**, 5075–5079.

View Article Online
DOI: 10.1039/D5LC00219B

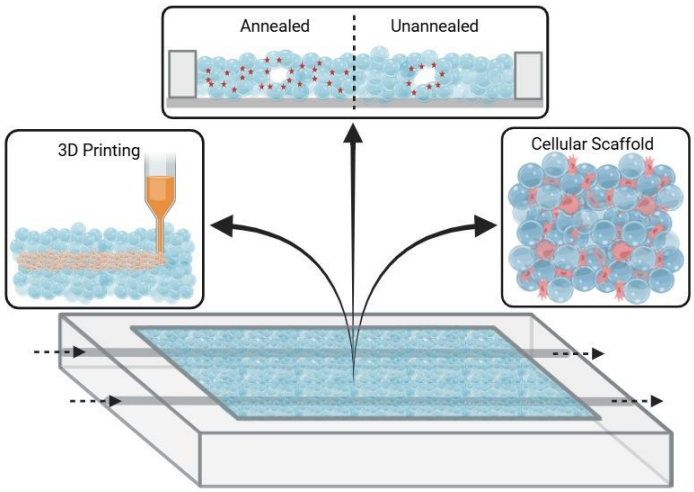

Figure 1: Schematic illustration of a granular hydrogel containing microfluidic device system that could have multiple channels, crosslinked or annealed, between microparticles within the granular hydrogel (indicated by red points in top insert) could be designed throughout the entire scaffold or be localized immediately adjacent to the channels in the hydrogel. With in the volume of the hydrogel between the channels, it would be possible to further define or modify the material structure via 3D printing. Cells might be included among the hydrogel microparticles, if desired.

View Article Online
DOI: 10.1039/D5LC00219B

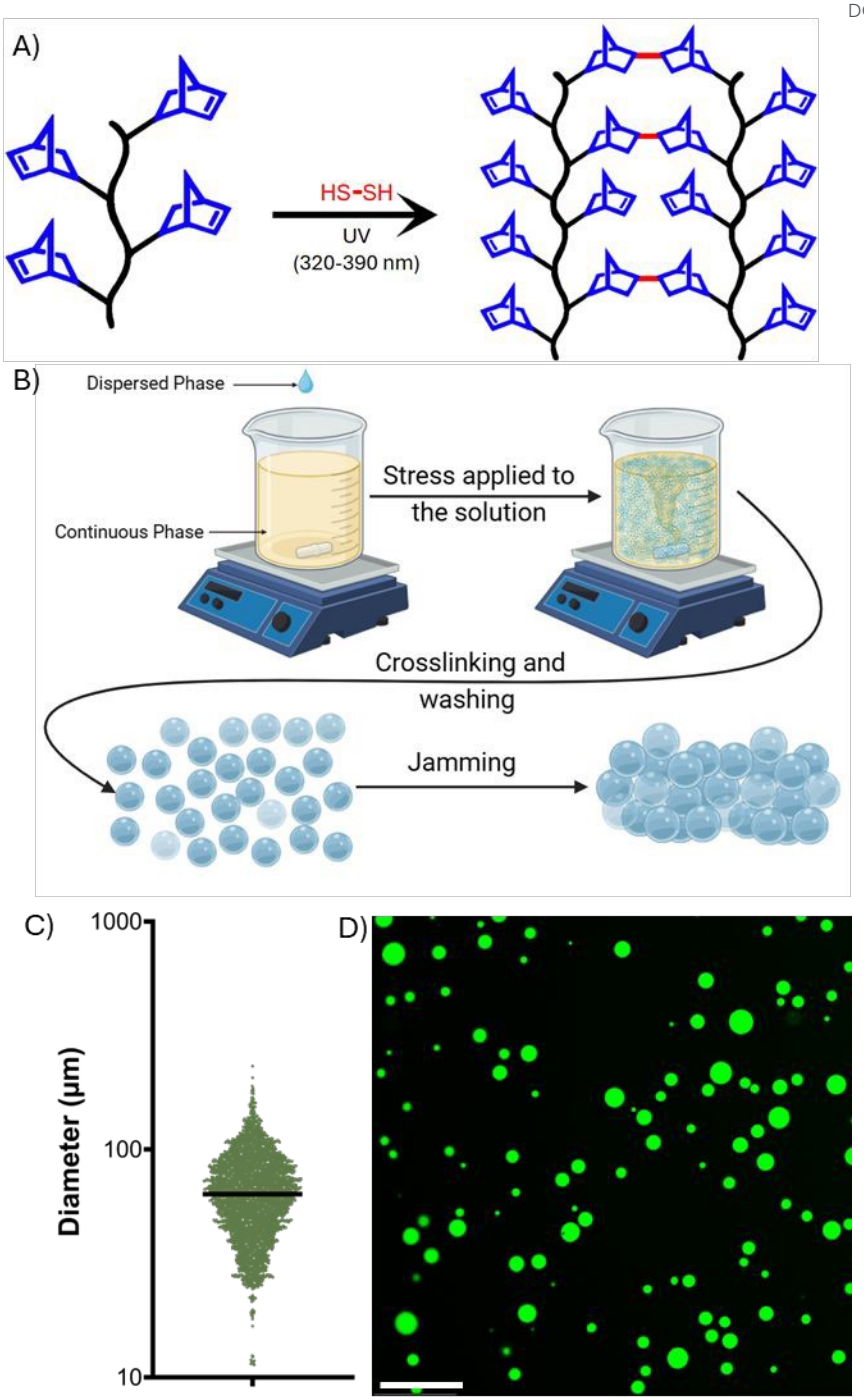

Figure 2: A) Hyaluronic acid (black) functionalized with norbornene groups (blue) and reacted with dithiol crosslinker (red) to form the hydrogel polymer network. B) Batch emulsification technique to fabricate hydrogel microparticles. C) Size distribution and D) representative image of NorHA hydrogel microparticles (scalebar 500 µm).

View Article Online
DOI: 10.1039/D5LC00219B

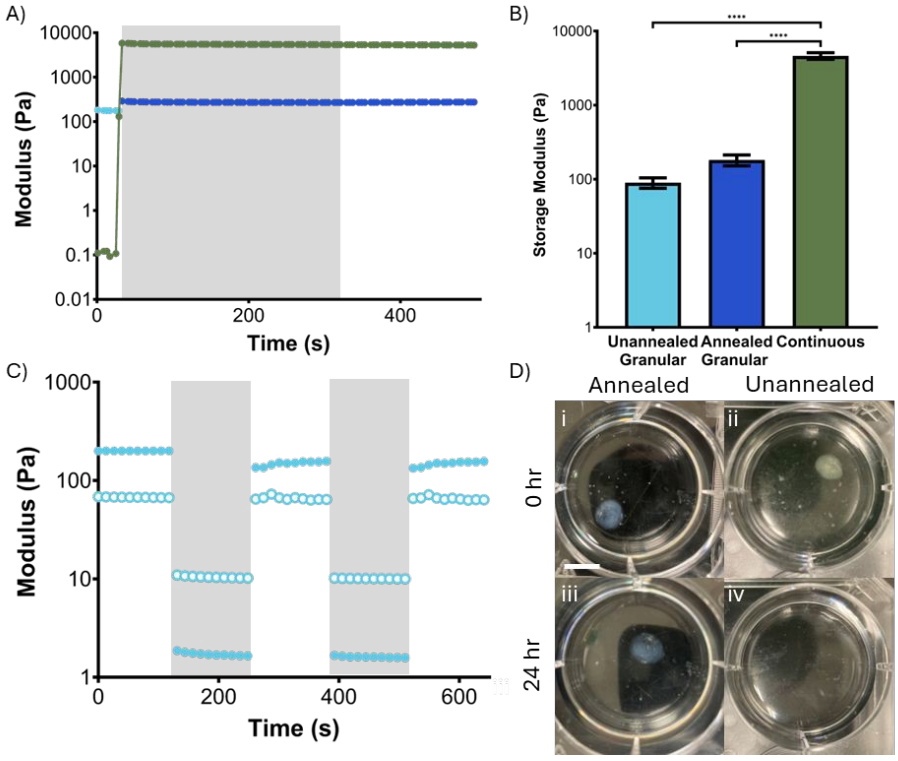

Figure 3: A) In situ rheology of the gelation of a NorHA continuous hydrogel (green) and granular hydrogel (light blue unannealed, dark blue annealed), the grey area represent the UV light on. B) Quantification of the storage modulus at 0.1 rad/s (n=3, $p \leq 0.0001$). C) Cyclic strain sweep alternating between high (white) and low (grey) strain of unannealed packed NorHA microparticles. D) Packed microparticles that are annealed (i) and not annealed (ii) together right after exposure to UV light and annealed and unannealed microparticles after 24 h (scalebar 20 mm).

View Article Online
DOI: 10.1039/D5LC00219B

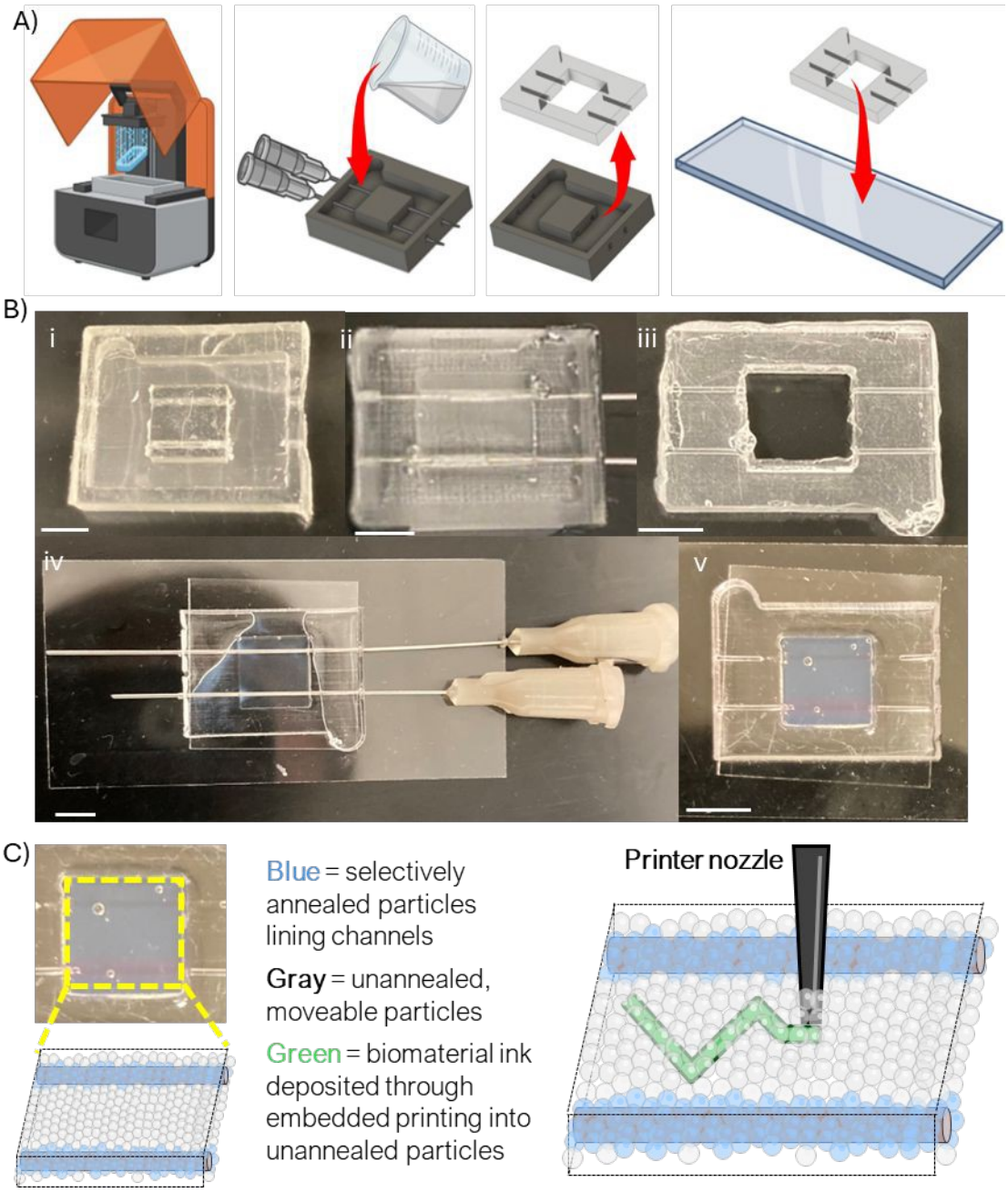

Figure 4: A) Device manufacturing process of fabricating the microfluidic device used here. B) 3D printed negative mold of the device (i), the mold loaded with PDMS (ii), the PDMS device (iii), the PDMS device plasma boned to a glass coverslip loaded with hydrogel solution ready to be crosslinked under UV light (iv), and the device after being crosslinked and having Rhodamine B injected into the channels (v) to help with visualization of them (scalebar 5 mm). C) Schematic illustration of selectively crosslinked material in Bv, with two stable channels lined by annealed particles (blue), surrounding a granular hydrogel bulk (gray particles between blue). A printer nozzle can move through these particles depositing biomaterial- and bioinks (green) within the unannealed particles (right).

View Article Online
DOI: 10.1039/D5LC00219B

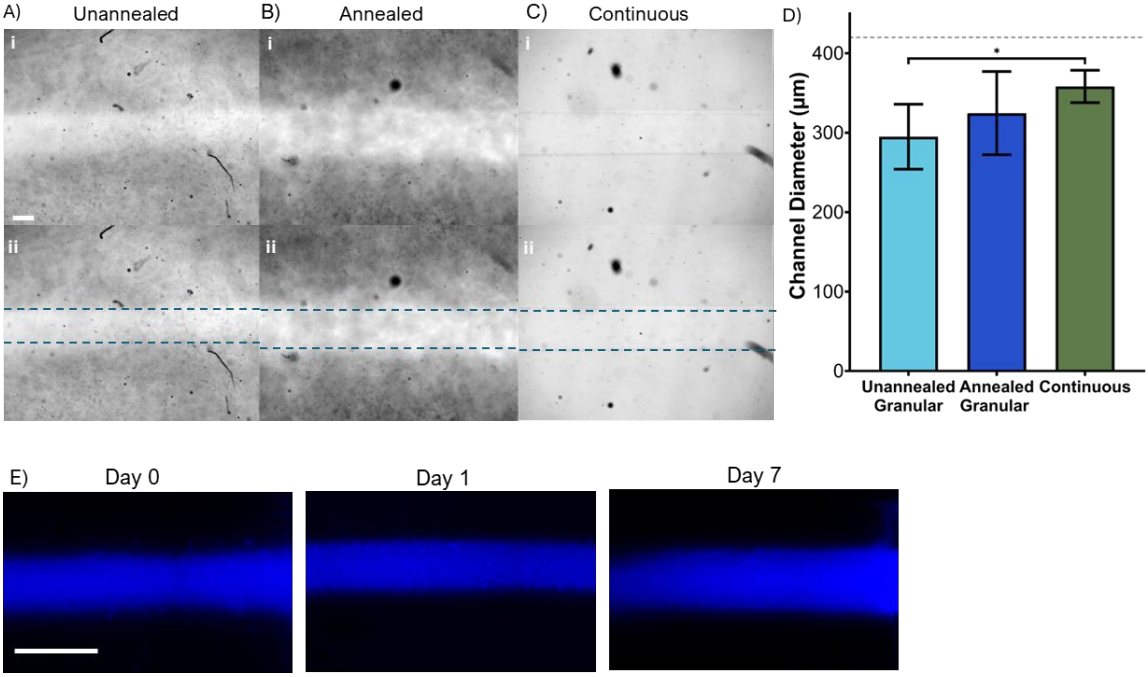

Figure 5: Brightfield images of channels after the templating needle was removed from A) the granular hydrogel selectively crosslinked along the channel ("unannealed"), B) the fully crosslinked granular hydrogel ("annealed"), and C) the continuous hydrogel (scale bar 200 µm). D) Quantification of the channel diameter where the grey dash line represents the needle diameter ($n = 3$, $p \leq 0.05$). E) Fluorescent images of channel in selectively annealed ('unannealed") granular hydrogel at day 0, day 1, and day 7 after initial channel formation (scalebar 1 mm).

View Article Online
DOI: 10.1039/D5LC00219B

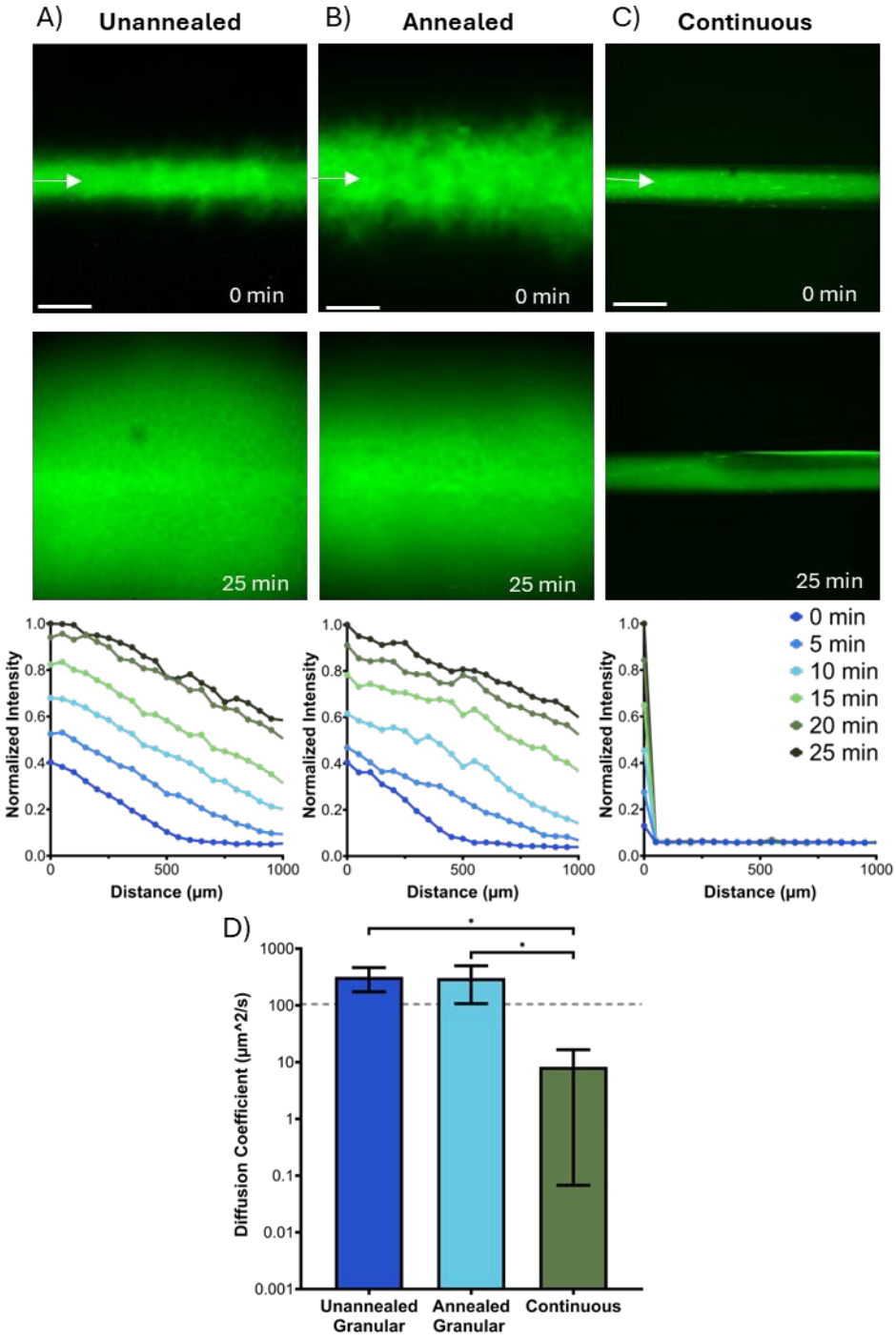

Figure 6: A-C) Representative images of FITC-albumin diffusing into the hydrogel from the channel at 0, and 25 mins for unannealed granular, annealed granular, and continuous hydrogel and the normalized intensity profiles of the fluorescent signal from the channel that where then used to calculate the diffusion coefficients (scalebar 500 μm). D) Calculated estimated diffusion coefficients of continuous, annealed granular, and unannealed granular hydrogel, the grey dash line is the diffusion coefficient of albumin in water at 37 °C (n = 3, $p \leq 0.05$).

View Article Online
DOI: 10.1039/D5LC00219B

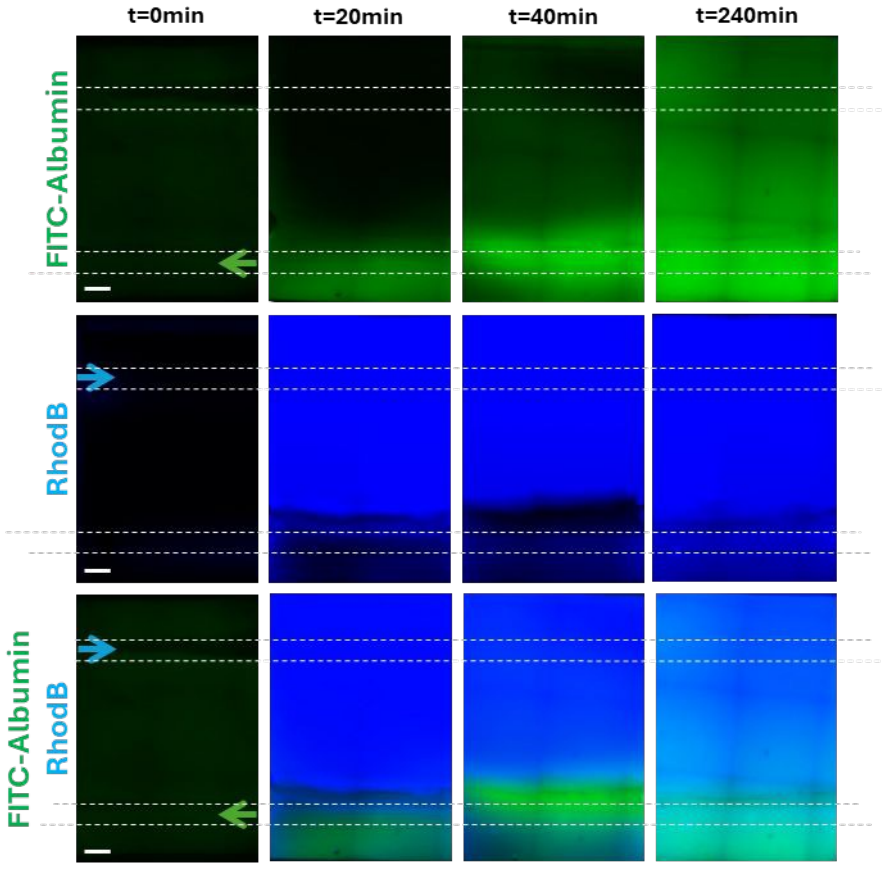

Figure 7: Anti-parallel flow of FITC-albumin (green) and rhodamine B (blue) within the device over time. Top row is FITC-albumin, middle row is rhodamine B, bottom row is rhodamine B and FITC-albumin overlay (scalebar = 500 μm).

View Article Online
DOI: 10.1039/D5LC00219B

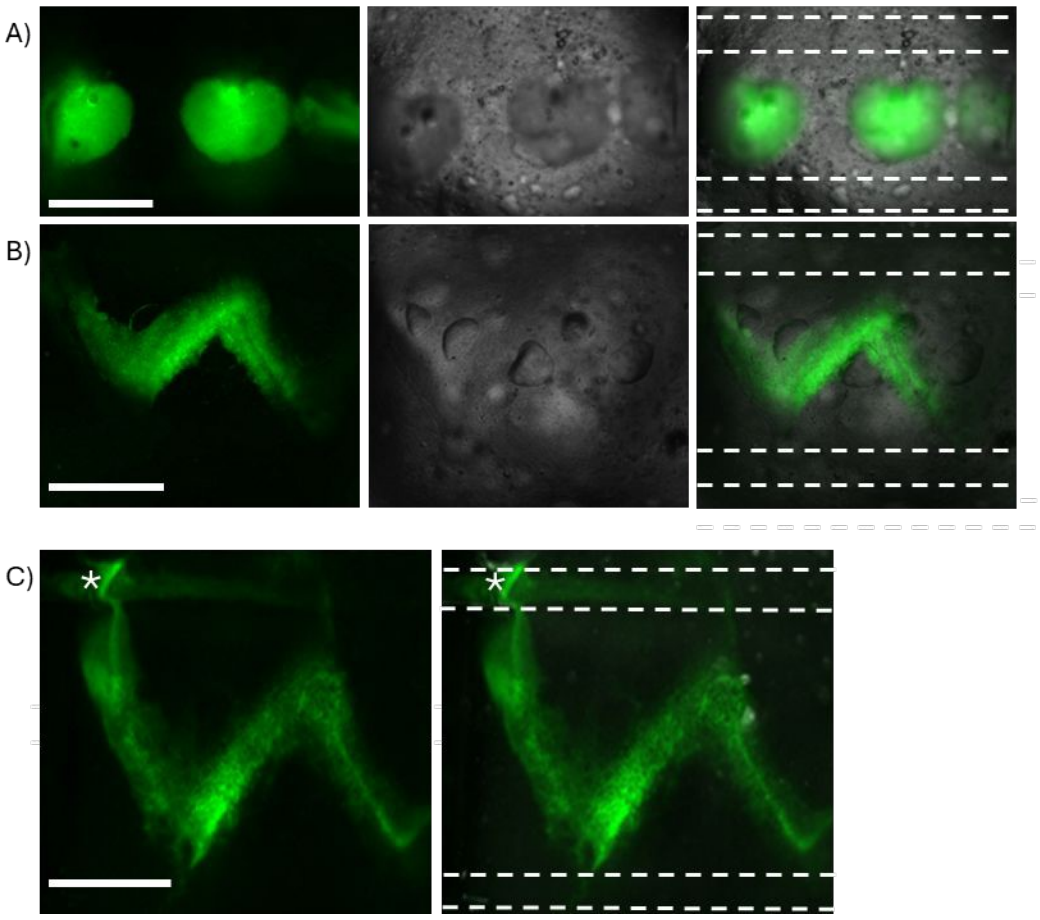

Figure 8: 3D printing of gelatin microparticles (green) into the NorHA microparticle support bath between two channels. Channel locations indicated by dotted lines. Complex material structures composed of (A) voxels and (B) a sawtooth pattern were established between channels in the device. (C) To help visualize the presence of the channels, gelatin melting during incubation at 37 °C could be seen flowing into a channel that is in contact with the printed structure (starred), evidencing patency of the adjacent channel and its support of transport (scalebars = 2 mm).

View Article Online
DOI: 10.1039/D5LC00219B

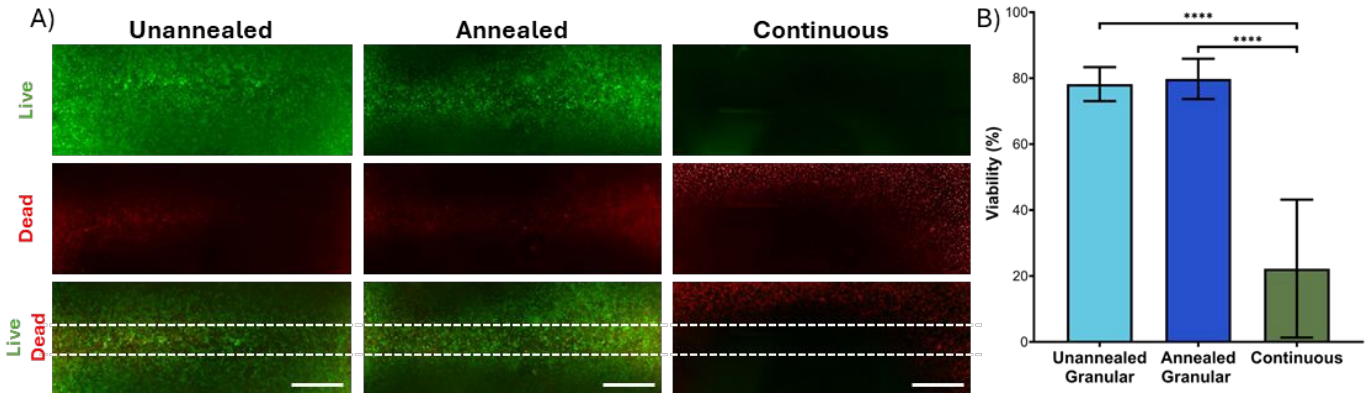

Figure 9: Channels and microporosity together support high cell viability. A) In channel-containing hydrogels within devices, HUVECs cultured 24 h were stained for viability (green) or cell death (red) in selectively crosslinked ("unannealed") granular hydrogels, fully annealed granular hydrogels, and continuous hydrogels (scalebar = 1 mm). B) Quantification of viability after 24 h show that granular hydrogels exhibited high viabilities close to 80%, while only 20% of the cells within continuous hydrogels were alive (n = 3, $p \leq 0.0001$).

View Article Online
DOI: 10.1039/D5LC00219B

Data Availability Statement

The data supporting these findings is available in Supplementary Information. Additional data is available upon request from the corresponding author.